ELSEVIER

Available online at www.sciencedirect.com

SCIENCE DIRECT®

International Journal of Solids and Structures 43 (2006) 3197–3212

INTERNATIONAL JOURNAL OF SOLIDS and STRUCTURES

www.elsevier.com/locate/ijsolstr

In-plane properties of composite laminates with through-thickness pin reinforcement

Craig A. Steeves, Norman A. Fleck *

Cambridge University, Engineering Department, Trumpington Street, Cambridge CB2 1PZ, UK

Received 11 February 2005; received in revised form 18 May 2005
Available online 5 July 2005

Abstract

Laminated fibre-reinforced composites can be reinforced by through-thickness pins to reduce their susceptibility to delamination. However, the presence of the pins creates resin pockets and disrupts the alignment of the fibres, and may thereby lead to a degradation of the in-plane strength of the composite. Experiments and numerical simulations show that the presence of through-thickness reinforcing pins decreases the tensile strength of the composite by 27%, and the compressive strength of the composite by at least 30%. It is also shown that the pattern in which the pins are inserted has a strong influence on the compressive strength. A pin pattern is identified in order to minimise fibre alignment disruption and thereby maximise the compressive strength.

Keywords: Compression test; Scanning electron microscopy; Polymer matrix composites; Finite element analysis; Microbuckling

1. Introduction

Laminated composites are notoriously susceptible to delamination. Through-thickness pins, known as 'z-pins', have been proposed to increase delamination strength and toughness (Freitas et al., 1996). These pins are made from structural materials such as pultruded carbon fibre–epoxy composite, glass fibre composite or titanium alloy. The z-pins comprise rods inserted in the through-thickness direction (the '*z*'-direction) of a laminated composite, and they serve to stitch the material together by a combination of friction and adhesion. The insertion process is as follows. Rods of diameter 0.1–1 mm are cut to a length of approximately 4 mm, with chamfered ends to improve the ease of insertion. They are inserted into a polymer foam

* Corresponding author. Tel.: +44 1223 332650; fax: +44 1223 332662.
E-mail address: naf1@eng.cam.ac.uk (N.A. Fleck).

0020-7683/$ - see front matter
doi:10.1016/j.ijsolstr.2005.05.017

carrier and arranged in a square pattern. The foam carrier is then placed on one face of an uncured composite laminate and an ultrasonic horn is used to drive the pins into the composite laminate. The laminate is air cooled in a freezer, allowing the excess pin material to be sheared off with a razor blade. Finally, the plate is autoclaved using the standard cure cycle for the composite laminate. This approach to through-thickness reinforcement offers an alternative to stitching, and can provide much higher areal densities of reinforcement.

A substantial literature exists on the mechanics of crack bridging by fibres. The Aveston–Cooper–Kelly (ACK) model, presented in Aveston and Kelly (1973), is an approximate elastic shear lag model for fibres reinforcing cracked ceramic materials. Budiansky et al. (1986) analysed the steady-state cracking strength of a brittle matrix reinforced with long fibres, and Budiansky and Amazigo (1989) then extended this model to the small-scale bridging of cracks in fibre-reinforced brittle materials. Mai and his co-workers (Shu and Mai, 1993; Hu and Mai, 1993; Jain and Mai, 1995; Dransfield et al., 1998; Jain et al., 1998) considered delamination-buckling of laminated composites with cracks opening in mixed mode. They used fracture mechanics concepts to predict the toughening due to crack bridging by both stitches and misaligned fibres. Cox (1999) developed a constitutive framework for a large-scale bridging model for a fibre or pin spanning a delamination crack opening in Mode II or in mixed mode. While this theory was developed for the stitching of composites, his model can also be applied to the case of z-pins.

A small literature already exists on the enhancement of out-of-plane properties (such as delamination toughness) due to the presence of z-pins. Freitas et al. (1996) presented strength data on a proprietary brand of z-pins, called Z-Fibers.[1] While they gave no quantitative information on the elevation in delamination resistance imparted by z-pins, they suggested that some degradation of the in-plane properties will occur. Barrett (1996) performed axisymmetric and three-dimensional finite element analysis of the delamination behaviour of carbon fibre–epoxy z-pins in a carbon fibre–epoxy laminate, including the effects of thermal expansion mismatch. Grassi et al. (2002) performed finite element computations of z-pinned reinforced laminates to determine in-plane moduli in tension and compression, and found that the knockdown in modulus was 7–10%. An analytical model for delamination of composites reinforced with z-pins was developed by Ratcliffe and O'Brien (2004). Cartie and Partridge (2005) carried out an experimental study on the improvement in delamination resistance offered by z-pins. Using double cantilever beams to measure the mode I delamination resistance, they found that z-pins gave a 6-fold to 25-fold increase in toughness as the areal density of pins was increased from 1% to 2%. Similar elevations in toughness were noted for mixed mode loading. No systematic studies have been found, however, on the knockdown of in-plane properties due to the presence of z-pins.

The current study examines the effect of z-pins upon the in-plane tensile and compressive stress versus strain responses of composite laminates. It is anticipated that the insertion of z-pins into a fibre laminate leads to both local stress concentrations and to fibre waviness. In tension, some reduction in strength is expected due to the stress concentrations. In compression, we expect that the stress concentrations and the fibre waviness will lead to a reduced fibre microbuckling strength of the laminate (Fleck, 1997). The experiments performed in this study confirm these conjectures. Finite element simulations are also reported for fibre microbuckling, and they reveal that the observed compressive strengths are consistent with the degree of as-manufactured fibre waviness.

2. Experimental procedure

The z-pins used in this study comprise pultruded composite rods of diameter 280 μm, made from BMI carbon fibre and an epoxy matrix. The following sequence of tests were performed on z-pinned

[1] Manufactured by Aztec Inc., 303 Bear Hill Road, Waltham, MA, 02154, USA.

unidirectional T300/914C and IMS/924C carbon fibre–epoxy laminates of thickness 1.5 mm. First, specimens with pins present and with pins absent ('control specimens') were tested in uniaxial tension to determine the effect of z-pins upon tensile strength. Second, pinned and control specimens were tested in uniaxial compression. Several z-pin configurations were used in the compression tests to explore the sensitivity of compressive strength to the geometric arrangement of pins. Third, z-pinned specimens were tested in uniaxial compression within the scanning electron microscope in order to observe the failure mechanisms.

2.1. Tensile tests

Unidirectional T300/914C laminates were reinforced with pultruded carbon-fibre/BMI rods of diameter 280 μm in a square configuration. The rods were spaced 1.75 mm centre-to-centre, giving an areal pin density of 2%. The principal directions of the pin arrangement were aligned with the specimen axes, such that the pin orientation angle is $\omega = 0°$, as defined in Fig. 1. All specimens were cut from the composite plates with a diamond-grit saw and ground to a width of 10 mm. Aluminium tabs of length 65 mm and thickness 1 mm were adhered to the specimens using Hexcel Redux 322 heat-cured epoxy sheet leaving a 50 mm gauge length. The recommended cure cycle was used: 1 h at 180 ° C under pressure, with suitable heating and cooling rates. The tensile specimens were loaded in displacement-control in a screw-driven test machine, using an axial strain rate of $1.67 \times 10^{-4}\,s^{-1}$. A clip gauge of gauge length 27.5 mm was attached to the specimen in order to measure the average axial strain within the pinned region. The specimens were loaded to failure, and both the load and average axial strain were logged at a sampling rate of 1 Hz.

2.2. Compression tests

Direct compression tests were performed on z-pinned specimens made from unidirectional T300/914C and IMS/924C carbon fibre–epoxy laminates in order to determine the effect of z-pin arrangement upon the in-plane compressive strength. The z-pins were arranged in a square configuration of spacing 3.5 mm or 1.75 mm at a pin orientation angle ω in the range 0–45°, as defined in Fig. 1.

There are three groups of test specimens as shown in Table 1. The first group comprises the control and pinned specimens of the unidirectional IMS/924C composite. The second group contains the control and pinned specimens of unidirectional T300/914C composite. In this group, the pinned specimens possess only a single row of three z-pins, aligned perpendicular to the axis of the specimen and placed at mid-length. The third group of specimens is also made from unidirectional T300/914C composite, but contains a grid of approximately 5×5 pins at an orientation of $\omega = 0°$, 23°, and 45°.

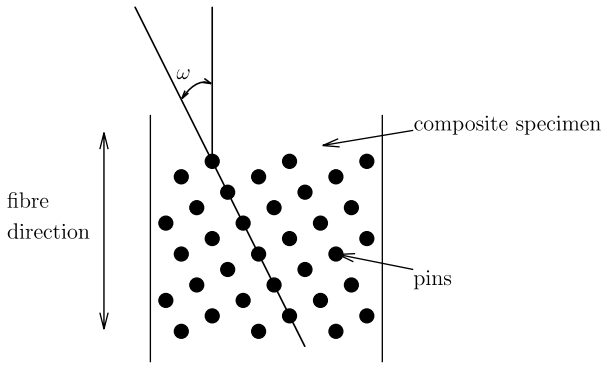

Fig. 1. Orientation of z-pin pattern. The orientation angle is ω.

Table 1
Summary of z-pinned compression specimens

Group	Composite system	Specimen set	Pin spacing (mm)	Orientation angle ω (deg)
1	UD IMS/924C	Control	n/a	n/a
		Pinned	1.75	0
2	UD T300/914C	Control	n/a	n/a
		One row	3.5	0
3	UD T300/914C	Control	n/a	n/a
		0°	1.75	0
		23°	1.75	23
		45°	1.75	45

The specimens of width 10 mm were cut from the composite laminates using a diamond-grit saw. Aluminium tabs, of length 65 mm and thickness 1 mm, were adhered to both ends of the specimens for gripping, leaving a 10 mm gauge length. Except for two groups of unpinned control specimens, 120 Ω strain gauges of length 1 mm were adhered in the axial direction to each face of the specimen, using cyanoacrylate adhesive. The strain gauges were coated with several layers of quick-drying liquid latex for protection, and were used to monitor both the axial strain and the degree of unwanted bending.

Uniaxial compression tests were performed on the three groups of specimens of Table 1 using a Celanese test rig. In this rig, a set of nested cones and cylinders grip the specimen with a pair of self-tightening jaws. The specimen is loaded by shear, eliminating the problem of end-brooming. The Celanese rig was placed in a screw-driven test machine, and the cross-head was displaced at a rate of 0.0083 mm s^{-1} until the specimen failed, giving a strain rate of approximately 1×10^{-4} s^{-1}. During each test, the load and strain gauges were logged automatically on a PC-based data logger; the axial strain was taken as the mean of the readings on the front and back face strain gauges. Videos were also taken of the gauge section in order to record the failure mode.

2.3. In situ scanning electron microscopy

Compression tests, performed in situ within the scanning electron microscope (SEM), can provide qualitative information about the nature of failure in the z-pinned specimens. The high stiffness of the test rig minimises the elastic energy stored within the test rig at peak load, and thereby minimises the degree of damage to the specimen post-peak load. This allows for the observation of damage evolution within the specimen.

The geometry of the specimens used for compression tests in the scanning electron microscope is shown in Fig. 2. Specimens of length 10 mm, width 4 mm and thickness 0.75 mm were cut from plates of IMS/924C composite reinforced with 280 μm diameter z-pins of centre-to-centre spacing 1.75 mm. The ends of the specimen were potted into brass grips with epoxy adhesive, and the specimen and grips were then gold-coated. A typical specimen, prior to testing, is shown in Fig. 3. Three z-pins are clearly visible in this specimen, with fibre waviness in the vicinity of each pin; there should be a fourth z-pin in the top right hand corner of this image, but it is missing; this illustrates the irregularity of the as-manufactured specimens.

Specimens were loaded by a screw-driven compression rig in situ within the scanning electron microscope (SEM) at a displacement rate of approximately 0.0033 mm s^{-1}, giving a compressive strain rate of 5.5×10^{-4} s^{-1}. Both video and still images were taken of the specimens as they were loaded to failure. After failure the specimens were removed from the electron microscope, re-coated with gold, and were then returned to the electron microscope for further examination.

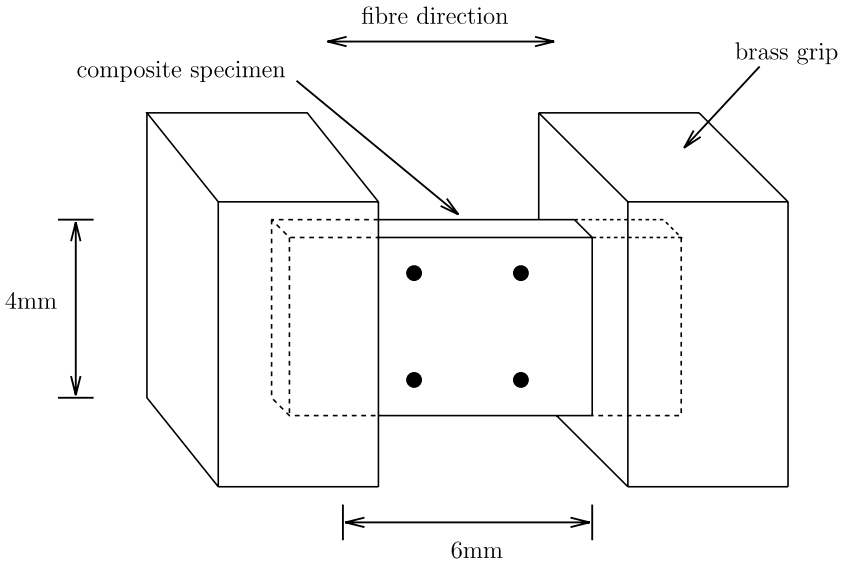

Fig. 2. Z-pinned specimen for compression testing in scanning electron microscope. The drawing is schematic and not to scale.

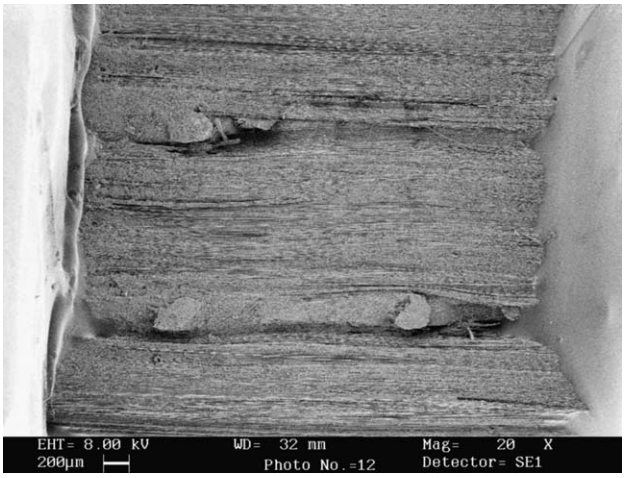

Fig. 3. Untested specimen of z-pinned laminate in scanning electron microscope. Three z-pins are evident, with a resin-rich pocket adjacent to each pin.

3. Results

3.1. Tensile tests

The tensile test results are summarised in Table 2. A two-sample *t*-test confirms that there is a significant difference in response for the pinned and control specimens: the average knockdown in strength is 27%. Fig. 4 shows typical stress–strain curves for these specimens. While both the pinned and control specimens have similar moduli, the pinned specimen splits earlier in the test than the control specimen, as shown in Fig. 4.

Table 2
Tensile strength for control and z-pinned specimens

	Control specimens strength (MPa)	Z-pinned specimens strength (MPa)
	1710	1290
	1700	1290
	1860	1280
Mean	1757	1286

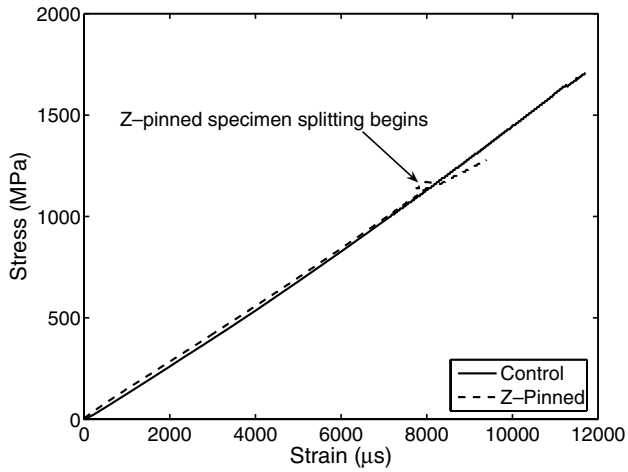

Fig. 4. Tensile stress–strain curves for typical pinned and unpinned specimens.

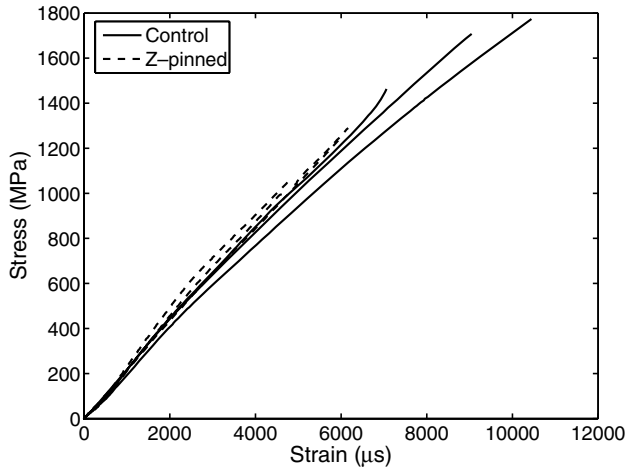

Fig. 5. Stress–strain curves for control and z-pinned specimens of unidirectional IMS/924C loaded in compression.

Ultimate failure is by fibre fracture. It is argued that the reduced longitudinal tensile strength of the pinned specimens is due to the stress concentration in the vicinity of the pins.

3.2. Compression tests

Three sets of compression tests were performed using the Celanese test rig, as summarised in Table 1. The uniaxial compressive stress versus strain responses of the IMS/924C specimens are shown in Fig. 5. Significant scatter in the peak strength is evident: this is characteristic of the compressive strength of composite laminates. Despite this scatter, the z-pinned specimens consistently failed at lower applied stress than the control specimens. The presence of z-pins degraded the mean compressive strength of the IMS/924C composite laminate by approximately 30%, see Table 3.

The compressive strengths of the T300/914C specimens are summarised in Table 4 for six specimens with a single row of z-pins (with $\omega = 0°$) and for six control specimens (with z-pins absent). The associated stress versus strain responses are given in Fig. 6 for each of the z-pinned specimens, and for two representative control specimens. It is evident that there is no significant effect of adding the single row of z-pins upon the compressive strength, to within material scatter. A two-sample t-test indicates that the two sets of specimens are not significantly different, with $p = 0.545$.

Four sets of T300/914C specimens were tested in order to explore the effect of orientation angle ω upon compressive strength: a set of control specimens without strain gauges, and three sets of z-pinned specimens with strain gauges adhered and $\omega = 0°$, 23°, and 45°. Stress–strain curves for the z-pinned specimens are shown in Fig. 7, while Table 5 summarises the compressive strengths for all z-pinned specimens tested, and for the four control specimens. All of the z-pinned specimens exhibited significantly lower compressive strength than the control specimens. A systematic drop in strength with increasing ω is evident. This trend is explained below in terms of the induced fibre waviness upon insertion of the z-pins.

3.3. In situ scanning electron microscopy

Specimens were compressed to failure in situ within the scanning electron microscope (SEM). In each case, failure was marked by a sharp drop in load, and by the appearance of a microbuckle band across the specimen. Fig. 8 shows the same specimen as in Fig. 3, but after failure. A microbuckle band is visible

Table 3
Compressive strengths of IMS/924C controls and specimens with a field of pins and $\omega = 0°$

	Control specimens strength (MPa)	Z-pinned specimens strength (MPa)
	1708	1235
	1463	1017
	1774	1290
Mean	1648	1181

Table 4
Compressive strengths of T300/914C controls and specimens with one row of z-pins

	Control specimens strength (MPa)	Z-pinned specimens strength (MPa)
	1329	1259
	1461	1299
	1473	1474
	1538	1520
	1314	1508
	1599	1412
Mean	1452	1412

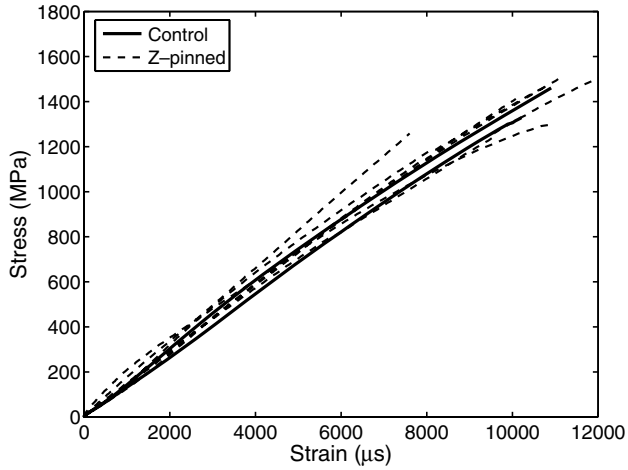

Fig. 6. Stress–strain curves for control and z-pinned specimens with one row of z-pins loaded in compression.

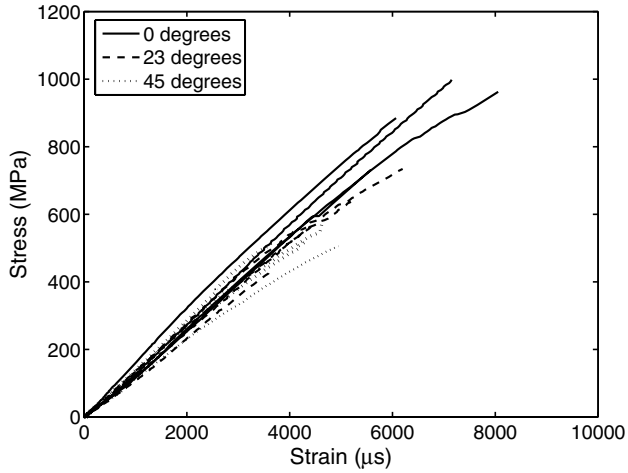

Fig. 7. Stress–strain curves for z-pinned T300/914C specimens with variable orientation angles loaded in compression.

Table 5
Compressive strengths of controls and z-pinned specimens with variable orientation angles

	Control specimens strength (MPa)	$\omega = 0°$ Strength (MPa)	$\omega = 23°$ Strength (MPa)	$\omega = 45°$ Strength (MPa)
	1745	885	637	506
	1439	963	436	580
	1670	998	561	518
	1311	731	734	517
Mean	1541	894	592	530

in the lower left hand side of the specimen. Fig. 9 is a close-up view of this microbuckle band, which extends away from the z-pin perpendicular to the fibre direction. Failure occurs almost instantaneously, making it impossible to determine from the video the exact location of microbuckle initiation.

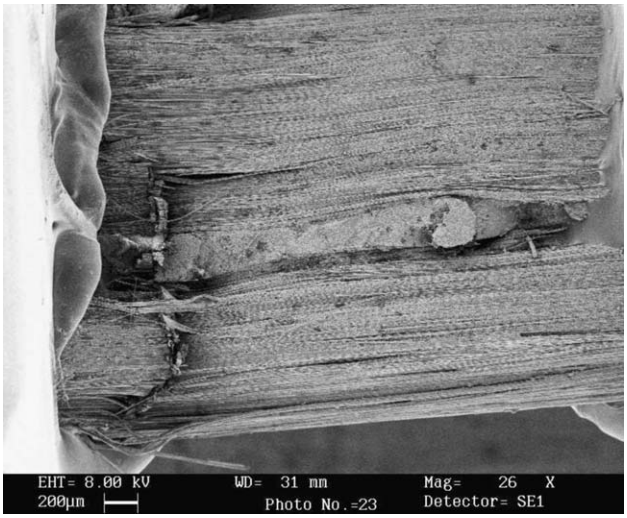

Fig. 8. Z-pinned specimen after testing in SEM.

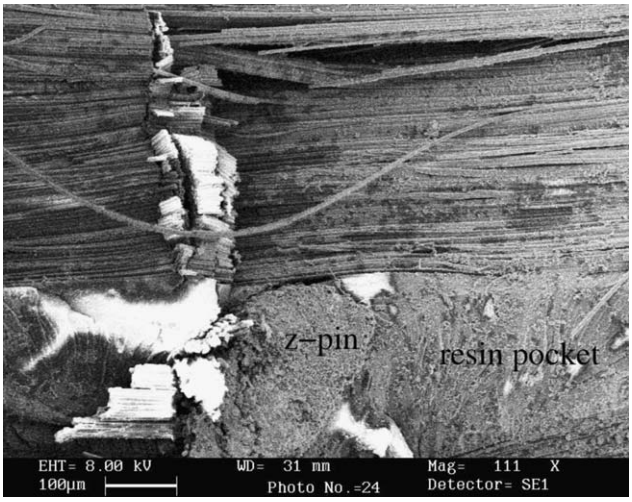

Fig. 9. Close up of microbuckle band near z-pin.

4. Image analysis of the IMS/924C specimens

It is well-established that the microbuckling strength of a fibre composite is dictated by the misalignment of the longitudinal fibres, see for example the review of Fleck (1997). Image analysis of the SEM digital images of the IMS/924C specimens provides a method for quantifying the fibre waviness distribution. The following section will describe a method developed by Creighton et al. (2001), hereafter called the CSC algorithm, which was used to characterise the composite laminates in this study. The results of this image analysis will then be presented.

4.1. Typical morphology

Fig. 10 shows a sketch of the typical distribution of fibre misalignment around a z-pin. The z-pin leads to two resin-rich pockets upon autoclaving: the fibres deflect around the z-pin and leave a gap in the composite. The misalignment of the deflected fibres is a maximum on the four flanks of the resin-rich pocket. In practice, fibres are not normally deflected symmetrically around the pin; irregularities in the pinning process and the random pre-existing fibre waviness tend to produce an asymmetric distributions of waviness.

In addition to deflection around a single pin, fibres may weave between successive z-pins. This phenomenon is sketched in Fig. 11; it may arise when the z-pin pattern is slightly distorted due to irregularities in the insertion process, or because of pre-existing misalignment in the 0° fibres. A typical example of weaving between adjacent z-pins is given in the SEM micrograph of Fig. 12. This weaving is significant because the associated fibre misalignment exceeds that due to symmetric fibre deflection around z-pins. Consequently, the microbuckling compressive strength is diminished.

4.2. Image analysis procedure

The CSC image analysis method takes digital images of the fibre composite as input. The image is divided into fields, and the local direction along which the pixel intensity is most highly correlated defines the fibre direction for that field. The distribution of fibre alignment for the composite laminate is then

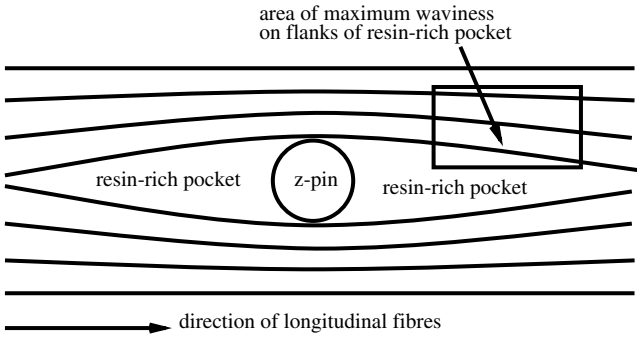

Fig. 10. Typical morphology of local area around z-pin.

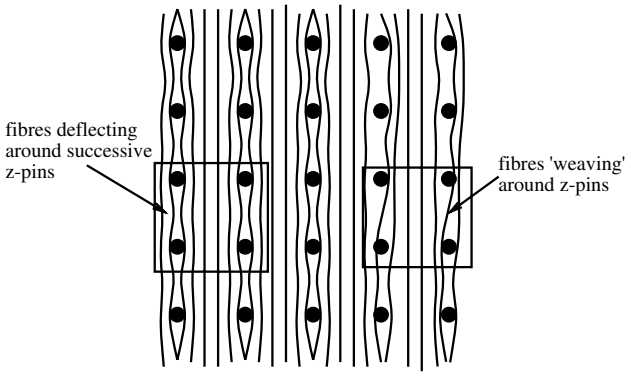

Fig. 11. Sketch of fibres deflecting around z-pins and 'weaving' through a field of z-pins.

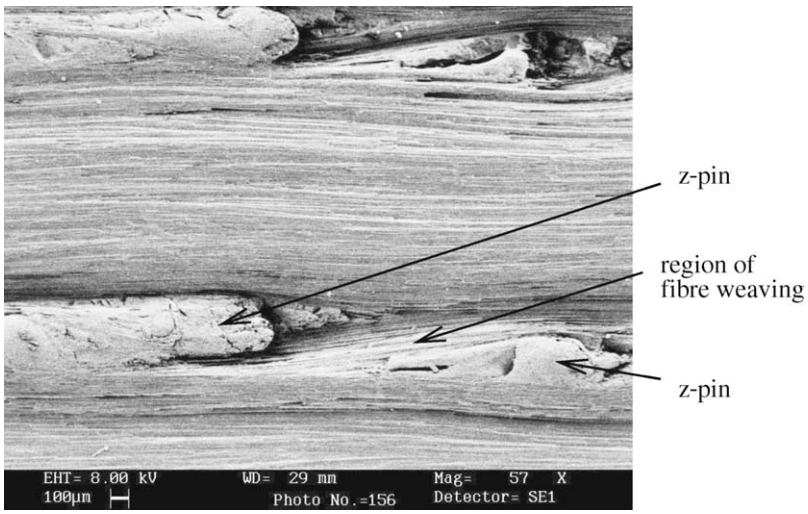

Fig. 12. Scanning electron microscope image of fibres 'weaving' between two z-pins.

assembled. SEM images of three different composite laminates were analysed. They were T300/914C laminates with a 1.75 mm square pattern of 280 μm diameter z-pins with orientation angles $\omega = 0°$, 23°, and 45° as listed in Table 1. The specimens were gold-coated and digital SEM images 2000 pixels by 1500 pixels were captured from each specimen and enhanced to increase the contrast. The resulting image was then used as the input for the CSC algorithm.

4.3. Results

Fig. 13 shows an SEM image of a laminate with z-pins at orientation angle 0° as used by the CSC algorithm to produce a contour map of fibre alignment. The area of the original image covered by the contour map is outlined with a dashed line. Note that the area of the resin-rich pocket and z-pin has been removed from the contour map as the alignment data for these areas have no significance. It is clear from the contour map that fibre misalignment of up to 14° occurs in two patches adjacent to the z-pin, while remote fibres show negligible misalignment. A similar procedure has been followed for the specimens with orientation angles of $\omega = 23°$ and 45°. The results of the image analysis were used as the input data for finite element calculations, as reported in the following section.

5. Finite element modelling

Shu and Fleck (1995) have developed the finite element code FLASH to predict the compressive strength of fibre composites containing elliptical patches of fibre waviness when subjected to compressive and shearing loads. This finite element model includes the role of initial fibre waviness and fibre bending stiffness by employing non-linear couple stress theory. The fibres and matrix are idealised as a ''smeared-out'' homogeneous solid with an additional degree of freedom which represents the rotation of the fibres. With increasing loading, FLASH tracks the evolution of fibre rotation and modifies the local anisotropic constitutive law, leading to instability and peak load at relatively small fibre rotations (Fleck and Shu, 1995). Liu and Fleck (1999) have updated FLASH to allow for arbitrary distributions of initial fibre waviness.

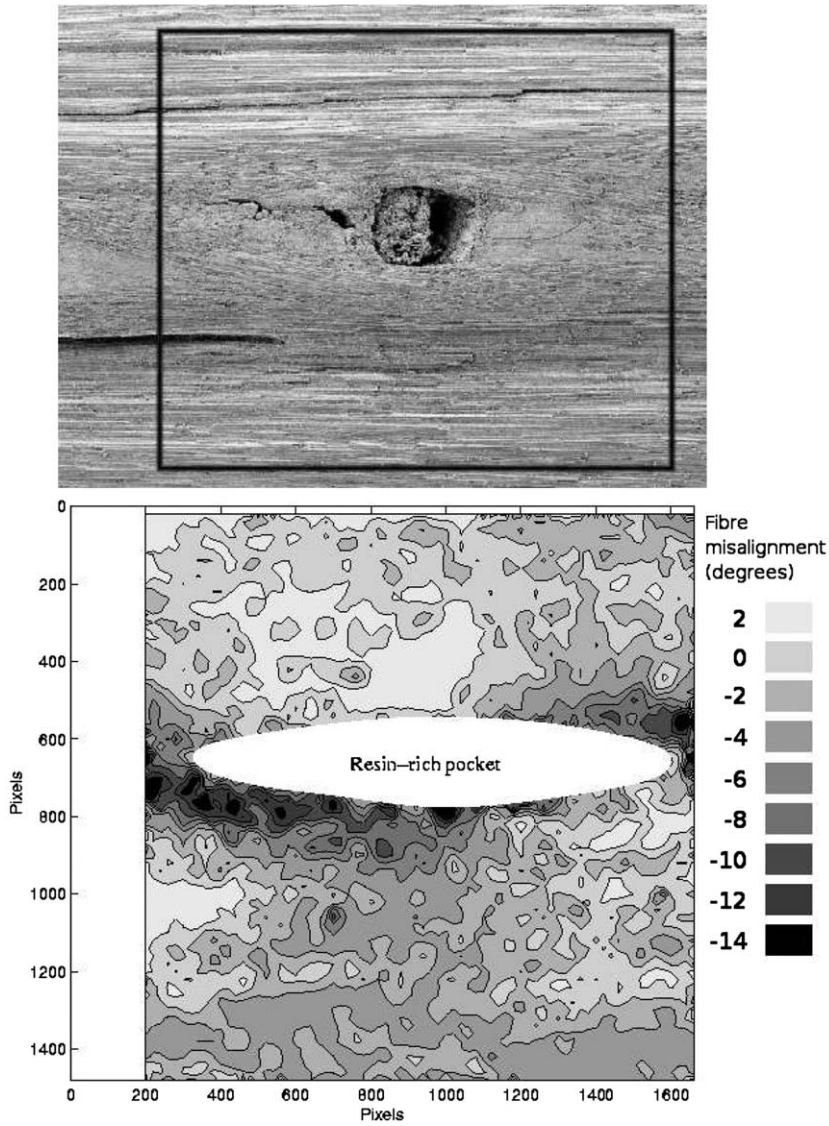

Fig. 13. Electron micrograph of z-pinned specimen, with contour map of fibre alignment angle. Dashed line shows the extent of the contour map.

In this study, a 2D finite element representation was made of the T300/914C laminates with a 1.75 mm square pattern of 280 μm diameter z-pins of orientation angles $\omega = 0°$, 23°, and 45°, as listed in Table 1. In all simulations, the composite is divided into unit cells of height 1.75 mm by width 1.75 mm, and only one cell is modelled using periodic boundary conditions. While this makes the computations less expensive, it assumes that all unit cells are identical; irregularities in manufacturing mean this is not strictly true. For these models, periodic boundary conditions are prescribed by applying compressive loading symmetrically to the specimen, and constraining three degrees of freedom to prevent rigid body translation and rotation. A typical mesh is shown in Fig. 14. Onto this mesh are imposed initial misalignment angles, taken from the

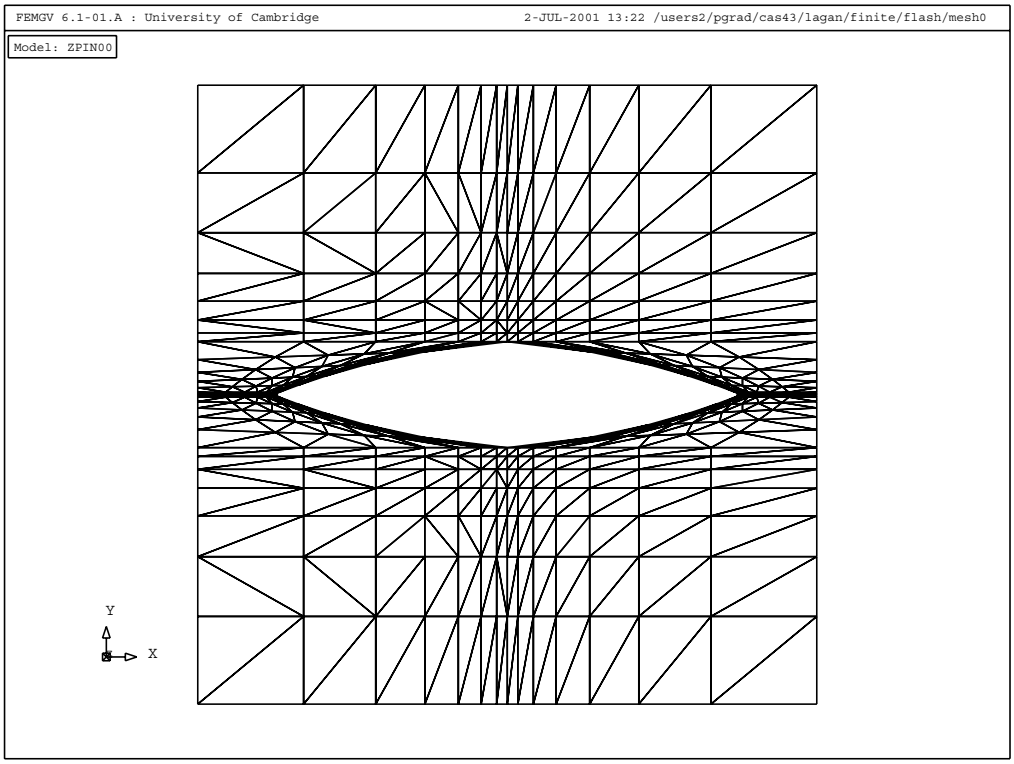

Fig. 14. Finite element mesh for z-pinned composite with 0° orientation angle.

results of the CSC algorithm as described above. Since fibre composites are known to be imperfection sensitive, it is important to use input data for the finite element simulations which are representative of the most serious defects in the real specimens. Here, fibre waviness measurements were taken around areas which appeared to be similar to regularly occurring serious defects in the composite. However, it is possible that these do not constitute the most serious defects. Consequently, the strengths predicted by the numerical simulations may be greater than the measured strengths.

The resin-rich pocket and the z-pin were modelled as voids within the material. This is justified because the matrix stiffness is much lower than that of the composite, and the resin-rich pocket cracks under low applied loads. Hence, the simulation includes the effect of both fibre misalignment and internal cavities. All meshes were generated using six-noded triangular plane-strain elements, and were refined near the resin pocket, and in the region of greatest fibre misalignment. The finite element code takes as input a fibre diameter of 7 μm and a longitudinal shear strength of $\tau_Y = 108$ MPa (Anon, 1997) for the T300/914C composite. Additional material parameters used by FLASH are the fibre volume fraction $v_f = 0.55$, longitudinal Young's modulus of the fibres $E_L = 117$ GPa, transverse shear modulus of the fibre material $G_f = 22$ GPa, composite transverse Young's modulus $E_T = 9$ GPa, composite shear modulus $G = 4.8$ GPa, and composite transverse compressive modulus $E_{TC} = 9.5$ GPa. The longitudinal shear stress τ is related to the shear strain γ by the familiar Ramberg–Osgood description $\frac{\gamma}{\gamma_Y} = \frac{\tau}{\tau_Y} + \alpha\left(\frac{\tau}{\tau_Y}\right)^n$ where $\gamma_Y = \tau_Y/G$ and the material parameters $\alpha = 3/7$ and $n = 3$ have been found to give an accurate description of the material response (Jelf and Fleck, 1992).

5.1. Finite element predictions

The finite element simulations predict the applied stress versus axial strain response and the evolution of fibre waviness with load. An increasing uniaxial compressive stress is applied to the model until a maximum stress is attained. This maximum is taken to be the compressive strength of the composite. After the peak load, the possibility of a sharp snap-back in the applied compressive stress versus average axial strain is included by an implementation of the Rik's algorithm. The simulations revealed that a snap-back in plastic buckling response does occur.

Figs. 15 and 16 compare the distribution of fibre misalignment in the z-pinned specimen before loading and after failure due to microbuckling, respectively. In order to emphasise the location of the microbuckle band, the calculation has been run beyond the peak load. The critical microbuckle band formed below and to the left of the z-pin in Fig. 16, as labelled. Upon comparison with the electron micrograph in Fig. 9, it is

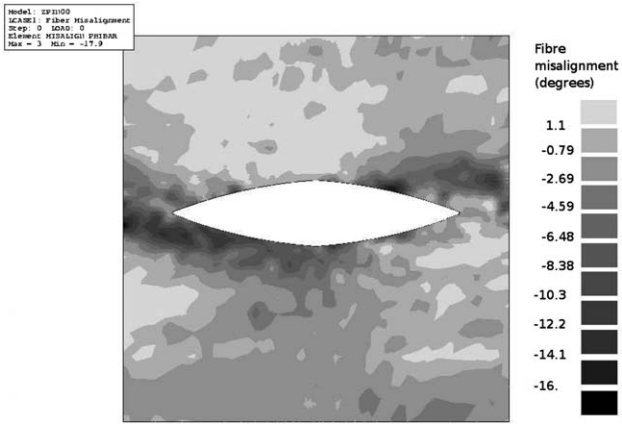

Fig. 15. Initial fibre alignment for numerical model of 0° orientation angle specimen.

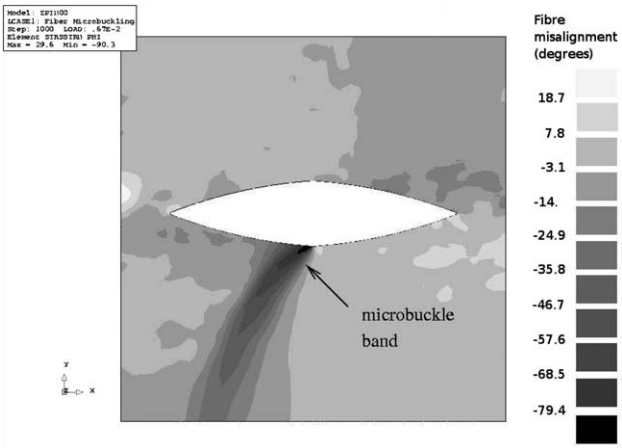

Fig. 16. Fibre alignment for numerical model of 0° orientation angle specimen after failure.

Table 6
Predicted and experimental strengths for specimens with variable orientation angle

Orientation angle ω (deg)	Measured strength (MPa)	Predicted strength (MPa)
0	894	887
23	592	788
45	530	643

clear that the location of the microbuckle failure predicted numerically is the same as that observed within the SEM. Further comparison with the initial distribution of fibre waviness in Fig. 15 shows that this failure location on the flank of the resin-rich pocket is in the region of large initial fibre misalignment, approximately 12°. Similarly, in the simulations of the specimens with ω equal to 23° and 45°, the microbuckle bands formed near the resin pockets in the regions of large initial fibre waviness.

The average values of observed strength and the predicted strengths from the finite element simulations are given in Table 6. Both the measured and predicted strengths reduce with increasing inclination ω, although the observed decline is the more marked. This may be a consequence of the difficulty of choosing images which correctly represent the most severe fibre misalignment in the specimens.

6. Concluding remarks

Experimental evidence and numerical simulations show that z-pins reduce the in-plane strength of composite laminates. The observed tensile strength of the unidirectional composites is reduced by approximately 27% while the compressive strength is reduced by at least 30% due to the presence of the z-pins.

The compression tests on the z-pinned specimens show a clear correlation between the knock-down of compressive strength and the degree of fibre misalignment. For example, the waviness induced by an inclined pattern of pins exceeds that for an aligned pattern of pins, and in turn exceeds that for a single row of pins; the measured compressive strength ranks in the inverse order. In principle, z-pins can be inserted in any desired pattern, and hence it may be possible to optimise the geometrical arrangement of the z-pins to reduce the degree of induced fibre waviness and thereby to maximise the in-plane compressive and tensile strengths.

The compressive strength of the z-pinned laminates is reduced by the misalignment of the fibres adjacent to the z-pins. The worst fibre misalignments are caused when fibres 'weave' through a field of z-pins, and 'weaving' is both more likely and more severe for 23° and 45° orientation angles than for the 0° orientation angle. As a consequence, the compressive strengths of the z-pinned composites are inversely related to the orientation angle. The 'weaving' effect dominates the compressive strength of the z-pinned laminates; when a single row of pins is inserted, so that no 'weaving' is possible, the compressive strength is not reduced from the unpinned compressive strength.

The combined procedure of image analysis using the Creighton–Sutcliffe–Clyne (CSC) algorithm in order to determine the distribution of fibre misalignment distribution and finite element simulations give predictions of compressive strength which follow the trends of the experimental data. However, fibre composites in compression are highly imperfection sensitive, and it is difficult to determine the most serious flaw inherent in a material by subjective means. In this study, the CSC algorithm was used to analyse the fibre waviness around a small number of selected z-pins. There are several limitations associated with this procedure: (i) the images are a two-dimensional slice of a three-dimensional solid; (ii) fibre waviness is not constant through the thickness of a laminate with the most severe flaws existing sub-surface; and (iii) only a small proportion of the z-pins can be analysed, possibly missing the worst flaws.

Acknowledgements

The authors would like to thank John Ellis of Hexcel Composites for prepregs and autoclaving facilities, Denis Cartié and Ivana Partridge of Cranfield University for access to z-pin preforms and insertion equipment, and Alan Heaver of CUED for the SEM images.

References

Anon, 1997. NCF stage 2 option 0 T300/914C material properties. Technical report, British Aerospace, Airbus Division.

Aveston, J., Kelly, A., 1973. Theory of multiple fracture of fibrous composites. Journal of Materials Science 8, 352–362.

Barrett, J.D., 1996. The mechanics of z-fiber reinforcement. Composite Structures 36, 23–32.

Budiansky, B., Amazigo, J.C., 1989. Toughening by aligned, frictionally constrained fibers. Journal of Mechanics and Physics of Solids 37 (1), 93–109.

Budiansky, B., Hutchinson, J.W., Evans, A.G., 1986. Matrix fracture in fiber-reinforced ceramics. Journal of Mechanics and Physics of Solids 34 (2), 167–189.

Cartie, D.D.R., Partridge, I., 2005. Delamination resistant laminates by z-fiber pinning. Part I: Manufacture and fracture performance. Composites Part A: Applied Science and Manufacturing 36 (1), 55–64.

Cox, B.N., 1999. Constitutive model for a fibre tow bridging a delamination crack. Mechanics of Composite Structures and Materials 6 (2), 117–138.

Creighton, C.J., Sutcliffe, M.P.F., Clyne, T.W., 2001. A multiple field image analysis procedure for characterisation of fibre alignment in composites. Composites Part A: Applied Science and Manufacturing 32 (2), 221–229.

Dransfield, K.A., Jain, L.K., Mai, Y.-W., 1998. On the effect of stitching in CFRPs—I. Mode I delamination toughness. Composites Science and Technology 58, 815–827.

Fleck, N.A., 1997. Compressive failure in fiber composites. Advances in Applied Mechanics 33, 43–117.

Fleck, N.A., Shu, J.Y., 1995. Microbuckle initiation in fibre composites: a finite element study. Journal of Mechanics and Physics of Solids 43 (12), 1887–1918.

Freitas, G., Fusco, T., Campbell, T., Harris, J., Rosenberg, S., 1996. Z-fiber technology and products for enhancing composite design. In: AGARD Conference Proceedings 590: Bolted/Bonded Joints in Polymeric Composites, Advisory Group for Aerospace Research and Development, pp. 17-1–17-8.

Grassi, M., Zhang, X., Meo, M., 2002. Prediction of stiffness and stresses in z-fibre reinforced composite laminates. Composites Part A: Applied Science and Manufacturing 33 (12), 1653–1664.

Hu, X.-Z., Mai, Y.-W., 1993. Mode I delamination and fibre bridging in carbon–fibre/epoxy composites with and without pval coating. Composites Science and Technology 46, 147–156.

Jain, L.K., Mai, Y.-W., 1995. Determination of mode II delamination toughness in stitched laminated composites. Composites Science and Techonology 55, 241–253.

Jain, L.K., Dransfield, K.A., Mai, Y.-W., 1998. On the effect of stitching in CFRPs—II. Mode II delamination toughness. Composites Science and Techonology 58, 829–837.

Jelf, P.M., Fleck, N.A., 1992. Compression failure mechanisms in unidirectional composites. Journal of Composite Materials 26 (18), 2706–2726.

Liu, D., Fleck, N.A., 1999. User's manual II for finite element code FLASH for fibre microbuckling. Technical Report CUED/C-MICROMECH/TR.29, Cambridge University Engineering Department, November.

Ratcliffe, J.G., O'Brien, T.K., 2004. Discrete spring model for predicting delamination growth in z-fiber reinforced DCB specimens. In: Proceedings of the American Society for Composites, Nineteenth Technical Conference, Atlanta, GA, 17–24 October 2004, American Society for Testing and Materials Committee D30.

Shu, D., Mai, Y.-W., 1993. Effect of stitching on interlaminar delamination extension in composite laminates. Composites Science and Technology 49, 165–171.

Shu, J.Y., Fleck, N.A., 1995. User's manual for finite element code for fibre microbuckling. Technical Report CUED/C-MATS/TR.224, University of Cambridge Department of Engineering, May.